

Thermalised dark radiation in the presence of PBH: ΔN_{eff} and gravitational waves complementarity

Nayan Das,^{1,*} Suruj Jyoti Das,^{1,†} and Debasish Borah^{1,‡}

¹*Department of Physics, Indian Institute of Technology Guwahati, Assam 781039, India*

Abstract

We study the possibility of detecting dark radiation (DR) produced by a combination of interactions with the thermal bath and ultra-light primordial black hole (PBH) evaporation in the early universe. We show that the detection prospects via cosmic microwave background (CMB) measurements of the effective relativistic degrees of freedom ΔN_{eff} get enhanced in some part of the parameter space compared to the purely non-thermal case where DR is produced solely from PBH. On the other hand, for certain part of the parameter space, DR which initially decouples from the bath followed by its production from PBH evaporation, can re-enter the thermal bath leading to much tighter constraints on the PBH parameter space. We also discuss the complementary detection prospects via observation of stochastic gravitational wave (GW) sourced by PBH density perturbations. The complementary probes offered by CMB and GW observations keep the detection prospects of such light degrees of freedom very promising in spite of limited discovery prospects at particle physics experiments.

*Electronic address: nayan.das@iitg.ac.in

†Electronic address: suruj@iitg.ac.in

‡Electronic address: dborah@iitg.ac.in

I. INTRODUCTION

The matter content in the present universe is dominated by dark matter (DM) as suggested by numerous astrophysics and cosmology based observations [1, 2]. While a fundamental particle with the required characteristics can give rise to DM, the dark sector in general can be much richer. For example, the dark sector can contain different light degrees of freedom, commonly referred to as dark radiation (DR) [3]. While their contribution to the overall energy budget of the present universe is negligible, they can have different phenomenological significance as well as detection prospects. For example, a very light scalar or gauge boson can give rise to sizeable self-interaction of DM having the potential to solve the small-scale structure issues of cold dark matter paradigm [4–6]. Other relativistic degrees of freedom may arise in different particle physics scenarios in the form of (pseudo) Goldstone boson, moduli fields, graviton, light sterile neutrinos, Dirac active neutrinos and so on.

Similar to radiation energy density at present epoch, these light relativistic degrees of freedom typically contributes negligibly to the total energy budget. In spite of that, cosmological observations can tightly constrain their abundance. Presence of dark radiation can be probed at cosmic microwave background (CMB) experiments. Existing data from CMB experiments like Planck constrain such additional light species by putting limits on the effective degrees of freedom for neutrinos during the era of recombination ($z \sim 1100$) as [2]

$$N_{\text{eff}} = 2.99^{+0.34}_{-0.33} \quad (1)$$

at 2σ or 95% CL including baryon acoustic oscillation (BAO) data. At 1σ CL it becomes more stringent to $N_{\text{eff}} = 2.99 \pm 0.17$. Similar bound also exists from big bang nucleosynthesis (BBN) $2.3 < N_{\text{eff}} < 3.4$ at 95% CL [7]. All these bounds are consistent with SM predictions $N_{\text{eff}}^{\text{SM}} = 3.044$ [8–10]. (Note that references [11–14] report slightly higher value of $N_{\text{eff}}^{\text{SM}}$ as 3.045.)¹ Future CMB experiment CMB Stage IV (CMB-S4) is expected reach a much better sensitivity of $\Delta N_{\text{eff}} = N_{\text{eff}} - N_{\text{eff}}^{\text{SM}} = 0.06$ [16], taking it closer to the standard model (SM) prediction. Similar precision measurements are also expected from other planned future

¹ A very recent paper [15] reports $N_{\text{eff}}^{\text{SM}} = 3.043$ by taking into account of the NLO correction to $e^+e^- \leftrightarrow \nu_L \bar{\nu}_L$ interactions along with finite temperature QED corrections to the electromagnetic plasma density and effect of neutrino oscillations.

experiments like SPT-3G [17], Simons Observatory [18] as well as CMB-HD [19].

If dark radiation has sizeable interactions with the SM bath, it can be thermalised in the early universe, followed by decoupling at some stage. Depending upon the decoupling temperature and internal degrees of freedom, such dark radiation can have very specific predictions for ΔN_{eff} which can either be ruled out by existing Planck data or can be probed at future experiments. On the other hand, if DR has feeble interactions with the SM bath, it will not be thermalised but can still be produced via freeze-in. The contribution to ΔN_{eff} in such a case depends upon the DR-SM coupling. Even in the absence of any direct coupling between SM and DR, it is still possible for the latter to be produced in the early universe purely due to gravitational effects. One such possibility arises when the early universe has a sizeable abundance of primordial black holes (PBH). Depending upon the initial abundance of PBH, such DR produced solely from PBH evaporation can contribute substantially to ΔN_{eff} [20, 21]. Similar works related to production of such light beyond standard model (BSM) particles including dark radiation from PBH evaporation and phenomenological implications can be found in [22–28] and references therein. In the presence of DR, entire PBH mass window in the ultra-light ballpark namely $\sim 0.1 - 10^8$ g can be probed in future CMB experiments while current Planck data ruling out certain PBH masses with large initial fractions.

Motivated by this, in the present work we consider a hybrid scenario where dark radiation can be produced both from the thermal bath as well as from PBH evaporation. While PBH can give an extra contribution to ΔN_{eff} , it can also dilute any initial ΔN_{eff} generated thermally. Additionally, depending upon DR-SM interactions, PBH evaporation can lead to re-thermalisation of DR as well, putting new constraints on PBH parameters not obtained in earlier works carried out in the absence of additional DR-SM interactions. We first show the results by considering different types of dark radiation with specific decoupling temperatures and corresponding ΔN_{eff} . To illustrate the issue of re-thermalisation we consider the DR to be in the form of light Dirac neutrinos (right chiral part) although the generic conclusions reached here are valid for other types of DR as well which have sizeable interactions with the SM bath. Assuming PBH to dominate the universe at early epochs such that the constraints from ΔN_{eff} is the strongest, we also show the prospects of gravitational waves (GW) complementarity in present and future experiments. The ultra-light PBH considered in our work can lead to GW production due to PBH density fluctuations keeping it in the

observable ballpark of mHz-kHz frequencies with peak amplitudes lying within reach of even LIGO-VIRGO as well as several planned experiments. We find interesting complementarity between ΔN_{eff} observations at CMB experiments and GW observations at present and near future GW detectors.

This paper is organised as follows. In section II, we briefly summarise the production of dark radiation from evaporating PBH. In section III, we consider DR production both from thermal bath and PBH evaporation with different examples of dark radiation. In section IV, we consider Dirac active neutrino as a specific example with effective four-Fermi type interactions with the SM bath and show the possibility of re-thermalisation and its implications. We discuss the gravitational waves complementarity in section V and finally conclude in section VI.

II. DARK RADIATION FROM PBH

Considering PBH to be formed in the early radiation dominated universe at a temperature, say T_{in} , the initial mass of PBH is related to the mass enclosed in the particle horizon and is given by [29–31]

$$m_{\text{in}} = \frac{4\pi}{3} \gamma \frac{\rho_{\text{R}}(T_{\text{in}})}{H^3(T_{\text{in}})}, \quad (2)$$

where $\gamma \approx 0.2$ [30], $\rho_{\text{R}}(T_{\text{in}})$ is the initial radiation density and H is the Hubble expansion rate. The temperature of a black hole can be related to its mass as [32]

$$T_{\text{BH}} = \frac{1}{8\pi G M_{\text{BH}}} \approx 1.06 \left(\frac{10^{13} \text{ g}}{M_{\text{BH}}} \right) \text{ GeV}. \quad (3)$$

PBH may dominate the energy density of the universe depending on their initial abundance, characterized by the dimensionless parameter

$$\beta = \frac{\rho_{\text{BH}}(T_{\text{in}})}{\rho_{\text{R}}(T_{\text{in}})}. \quad (4)$$

Once PBH form², they lose mass through Hawking evaporation at a rate given by [38]

$$\frac{dM_{\text{BH}}}{da} = -\frac{\epsilon(M_{\text{BH}})\kappa}{aH} \left(\frac{1 \text{ g}}{M_{\text{BH}}}\right)^2. \quad (5)$$

Here a is the scale factor and $\kappa = 5.34 \times 10^{25} \text{ g s}^{-1}$ [21]. Because of only gravitational effects, production of all particles takes place, regardless of their interaction with other particles. The evaporation function $\epsilon(M_{\text{BH}})$ [21] contains contributions from both SM and BSM particles. The temperature of the thermal plasma when the PBH have completely disappeared can be found by integrating Eq. (5), and can be written as [39]

$$T_{\text{ev}} \simeq \left(\frac{9g_*(T_{\text{BH}})}{10240}\right)^{\frac{1}{4}} \left(\frac{M_{\text{P}}^5}{m_{\text{in}}^3}\right)^{\frac{1}{2}}, \quad (6)$$

where M_{P} denotes the reduced Planck mass.

For the early universe to be black hole dominated, the initial energy density of PBH should satisfy [21]

$$\beta \geq \beta_{\text{crit}} \equiv 2.5 \times 10^{-14} \gamma^{-\frac{1}{2}} \left(\frac{M_{\text{BH}}(T_{\text{in}})}{10^8 \text{ g}}\right)^{-1} \left(\frac{\epsilon(M_{\text{BH}}(T_{\text{in}}))}{15.35}\right)^{\frac{1}{2}}. \quad (7)$$

Since PBH evaporation produces all particles, including radiation that can disturb the successful predictions of BBN, we require $T_{\text{ev}} > T_{\text{BBN}} \simeq 4 \text{ MeV}$. This can be translated into an upper bound on the PBH mass. On the other hand, a lower bound on PBH mass can be obtained from the CMB bound on the scale of inflation [40]: $H_I \equiv H(T_{\text{in}}) \leq 2.5 \times 10^{-5} M_{\text{P}}$, where $H(T_{\text{in}}) = \frac{1}{2t_{\text{in}}}$ with $t(T_{\text{in}}) \propto m_{\text{in}}$. Using these BBN and CMB bounds together, we have a window³ for allowed initial mass for ultra-light PBH that reads $0.1 \text{ g} \lesssim m_{\text{in}} \lesssim 4 \times 10^8 \text{ g}$. We consider this allowed mass range of ultra-light PBH in the context of dark radiation. For simplicity, we consider a monochromatic mass function of PBHs implying all PBHs to have identical masses. Additionally, the PBHs are assumed to be of Schwarzschild type without any spin and charge.

Now, if there exist any light BSM degrees of freedom or dark radiation, they can be produced directly from evaporating PBH, contributing to the effective number of relativistic

² Since our primary motive is to explore the effect of PBH on dark radiation, in this work we remain agnostic about the formation mechanism of PBH. PBH with our desired mass range and initial energy density can be formed through several mechanisms, say from inflationary perturbations [33–35], Fermi-ball collapse [36], loop quantum gravity [37] etc.

³ The range of PBH masses in this window remains typically unconstrained [30].

degrees of freedom N_{eff} defined as

$$N_{\text{eff}} = \frac{8}{7} \left(\frac{11}{4} \right)^{4/3} \left(\frac{\rho_R - \rho_\gamma}{\rho_\gamma} \right), \quad (8)$$

where ρ_R, ρ_γ denote total radiation and photon densities respectively. In order to track the evolution of the energy densities, we need to consider the following set of Boltzmann equations [21]

$$\frac{d\rho_{\text{BH}}}{da} + 3\frac{\rho_{\text{BH}}}{a} = \frac{1}{M_{\text{BH}}} \frac{dM_{\text{BH}}}{da} \rho_{\text{BH}}, \quad (9)$$

$$aH \frac{d\rho_R}{da} + 4H\rho_R = -\frac{\epsilon_R(M_{\text{BH}})}{\epsilon(M_{\text{BH}})} \frac{aH}{M_{\text{BH}}} \frac{dM_{\text{BH}}}{da} \rho_{\text{BH}}, \quad (10)$$

$$a \frac{d\rho_X^{\text{BH}}}{da} + 4\rho_X^{\text{BH}} = -\frac{\epsilon_X(M_{\text{BH}})}{\epsilon(M_{\text{BH}})} \frac{a}{M_{\text{BH}}} \frac{dM_{\text{BH}}}{da} \rho_{\text{BH}}. \quad (11)$$

Here, ρ_X^{BH} denotes energy density of a light species X produced solely from the evaporation of PBH. The ϵ_R and ϵ_X are the evaporation functions of SM particles and X species respectively. The combined evaporation function is denoted by $\epsilon = \epsilon_R + \epsilon_X$. The Hubble parameter H entering in the above equations is given by

$$H = \sqrt{\frac{\rho_{\text{BH}} + \rho_{\text{SM}} + \rho_X}{3M_{\text{P}}^2}}. \quad (12)$$

Since entropy is not conserved due to PBH evaporation, we track the evolution of the thermal bath separately through the equation given by

$$\frac{dT}{da} = -\frac{T}{\Delta} \left(\frac{1}{a} + \frac{\epsilon_{\text{SM}}(M_{\text{BH}})}{\epsilon(M_{\text{BH}})} \frac{1}{M_{\text{BH}}} \frac{dM_{\text{BH}}}{da} \frac{\rho_{\text{BH}}}{4(\rho_{\text{SM}} + \rho_X)} \right), \quad (13)$$

where

$$\Delta = 1 + \frac{T}{3g_{*s}(T)} \frac{dg_{*s}(T)}{dT}. \quad (14)$$

The extra relativistic degrees of freedom, ΔN_{eff} is defined as

$$\Delta N_{\text{eff}} = \frac{\rho_X(T_{\text{eq}})}{\rho_{\nu_{L,1}}(T_{\text{eq}})}. \quad (15)$$

Here $\rho_{\nu_{L,1}}(T_{\text{eq}})$ denotes the energy density of one species of SM neutrinos at the time of matter-radiation equality. In terms of energy densities at the time of PBH evaporation, the above expression turns out to be [21]

$$\Delta N_{\text{eff}}^{\text{BH}} = \left\{ \frac{8}{7} \left(\frac{4}{11} \right)^{-\frac{4}{3}} + N_{\text{eff}}^{\text{SM}} \right\} \frac{\rho_X(T_{\text{ev}})}{\rho_R(T_{\text{ev}})} \left(\frac{g_*(T_{\text{ev}})}{g_*(T_{\text{eq}})} \right) \left(\frac{g_{*s}(T_{\text{eq}})}{g_{*s}(T_{\text{ev}})} \right)^{\frac{4}{3}}, \quad (16)$$

where $N_{\text{eff}}^{\text{SM}} = 3.044$ and $\rho_X(T_{\text{ev}}), \rho_R(T_{\text{ev}})$ denote energy density of species X and SM after PBH evaporation respectively. The relativistic degrees of freedom in energy and entropy densities are denoted by g_*, g_{*s} respectively.

Now, in the case when PBH dominates the energy density of the universe at some epoch, Eq. (16) simplifies into

$$\Delta N_{\text{eff}}^{\text{BH}} = 13.714 \times \frac{\epsilon_X(M_{\text{BH}})}{\epsilon(M_{\text{BH}})} \frac{g_*(T_{\text{ev}})}{g_{*s}(T_{\text{ev}})^{\frac{4}{3}}}. \quad (17)$$

From the above equation, we can see that ΔN_{eff} remains constant for those values of PBH mass for which PBH evaporate before the electroweak scale since g_*, g_{*s} remains constant at high temperatures. As we keep on increasing the PBH mass further, ΔN_{eff} keeps on increasing. In the left panel of Fig. 1, we show the variation of ΔN_{eff} with the initial PBH mass m_{in} , for three different types of DR which includes right chiral part of Dirac active neutrinos ν_R , massless gauge boson (MGB) and Goldstone boson (GB). The current 2σ bound from Planck 2018 [41] and the future sensitivity of CMB-S4 [16] are also shown in the same figure.

III. THERMALISED DARK RADIATION IN THE PRESENCE OF PBH

If we consider the extra relativistic species to have interactions with the SM bath, ΔN_{eff} would receive a thermal contribution which depends on the temperature at which the thermal species decouple from the bath namely T_{dec} . It can be written as [42]

$$\Delta N_{\text{eff}}^{\text{th}} = 0.0267 \times f n_X g_X \left(\frac{106.75}{g_{*s}(T_{\text{dec}})} \right)^{4/3}, \quad (18)$$

where g_X, n_X is the internal spin degree of freedom of X and number of different species of type X respectively. f takes the value of $7/8$ for fermion and 1 for boson. T_{dec} denotes the decoupling temperature of the thermalised species. In the right panel of Fig. 1, we show the corresponding ΔN_{eff} by considering DR to be of thermal origin only. The x-axis denotes the decoupling temperature T_{dec} of DR from the thermal bath. As expected, a lower decoupling temperature leads to a larger contribution to ΔN_{eff} .

As we will see, in the presence of PBH, the total contribution to ΔN_{eff} from thermalised DR is decided by the interplay between the thermal and the non-thermal contribution. Interestingly, the total contribution depends on when the PBH evaporates relative to the

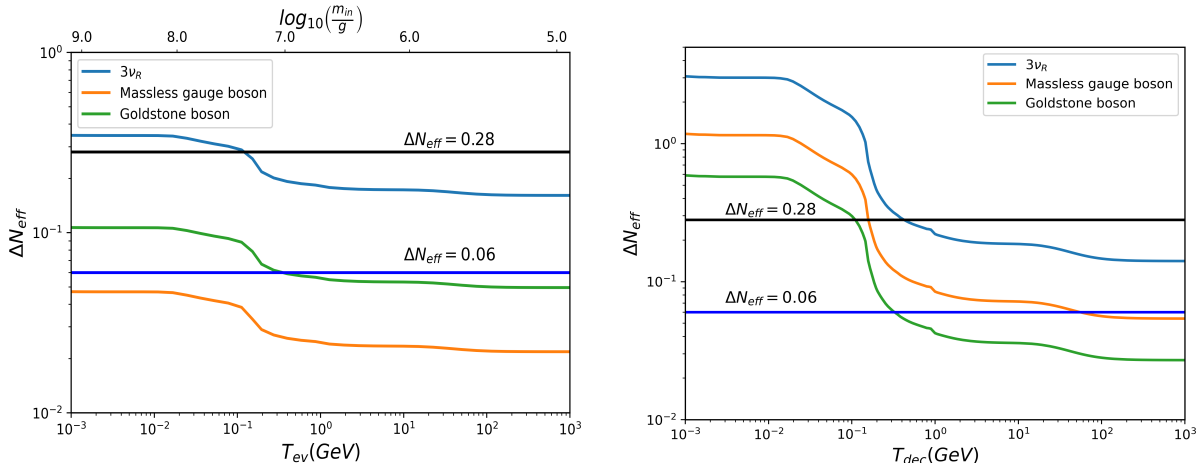


FIG. 1: *Left panel:* Variation of non-thermal contribution to ΔN_{eff} coming from PBH, with T_{ev} (or m_{in}), for different species. *Right panel:* Variation of thermal contribution to ΔN_{eff} with T_{dec} for different species.

decoupling temperature of the thermalised species. Depending on the initial fractional energy density (β) and the initial mass (m_{in}) of PBH at the time of formation, we can broadly divide our study into two categories: (A) PBH dominates the energy density of the universe at some epoch, and (B) PBH never dominates the energy density of the universe. These two possibilities lead to different observational consequences, which we discuss below.

A. PBH domination

The evaporation of PBH will produce all the SM particles along with DR. In the hybrid scenario considered here, DR can be produced gravitationally from PBH as well as from the SM bath by virtue of non-standard DR-SM interactions. Therefore, we can think of the total contribution to the extra number of relativistic species, ΔN_{eff} as the contribution from DR emitted from PBH and the already existing thermal counterpart, which was thermalised followed by decoupling from the thermal bath.

The decoupling temperature of extra light species, X depends on its coupling with SM particles. A smaller value of coupling can lead to an early decoupling. In such a scenario, the duration between decoupling and PBH evaporation can be quite long. Thus, to begin with, we neglect the interaction between the decoupled X and X produced from PBH. So, both

decoupled and light species from PBH can be treated as different species while considering their individual contribution to ΔN_{eff} . In a follow-up section, we explicitly consider a specific type of DR namely Dirac type active neutrinos with four-Fermi type interactions of right chiral part with the SM and study the validity of this assumption. On the other hand, for a larger value of DR-SM coupling, the PBH evaporation can occur much before the decoupling of light species, X . In that case, the emitted X from PBH will be thermalised completely with the SM bath, and both emitted and preexisting thermal X will behave as a single species.

Here, we make an estimate of ΔN_{eff} in the two limits discussed above. The evaporation temperature of PBH is connected to the initial PBH mass m_{in} through Eq. (6). Assuming that the species X decouples at the same temperature as PBH evaporation, we can draw the solid red line in Fig. 2 corresponding to $T_{\text{ev}} = T_{\text{dec}}$. Now, depending upon the values of its coupling with SM and m_{in} , we can have the two different scenarios, i.e. either $T_{\text{ev}} > T_{\text{dec}}$ (above the red line) or $T_{\text{ev}} < T_{\text{dec}}$ (below the red line). We discuss the dynamics for these two cases below.

1. PBH evaporation before decoupling of thermalised DR

We first consider the scenario, where the PBH evaporates earlier than the decoupling of thermalised species X . In such a case, the species X produced from PBH evaporation will also get thermalised. Therefore, the contribution to ΔN_{eff} comes only from the thermalised X , and is given by Eq. (18). For example, if X is considered to be the right chiral parts of Dirac active neutrinos, this equation reduces to

$$\Delta N_{\text{eff}} \simeq 0.027 \times 2 \times 3 \times \frac{7}{8} \left(\frac{106.75}{g_*(T_{\text{dec}})} \right)^{4/3} \simeq 0.14175 \times \left(\frac{106.75}{g_*(T_{\text{dec}})} \right)^{4/3}. \quad (19)$$

Thus, ΔN_{eff} becomes independent of m_{in} . For decoupling temperature $T_{\text{dec}} \lesssim 500$ MeV, ΔN_{eff} is more than 0.28, the current Planck bound at 2σ level. This is indicated by the region above the solid blue line in Fig. 2. A larger decoupling temperature reduces the contribution to N_{eff} . Note that this also requires a smaller value of PBH mass to make sure that PBH evaporates earlier compared to the decoupling epoch. Above a certain value of T_{dec} , the contribution to ΔN_{eff} saturates at a value of 0.14, indicated by the triangular region between solid green and solid red lines of Fig. 2.

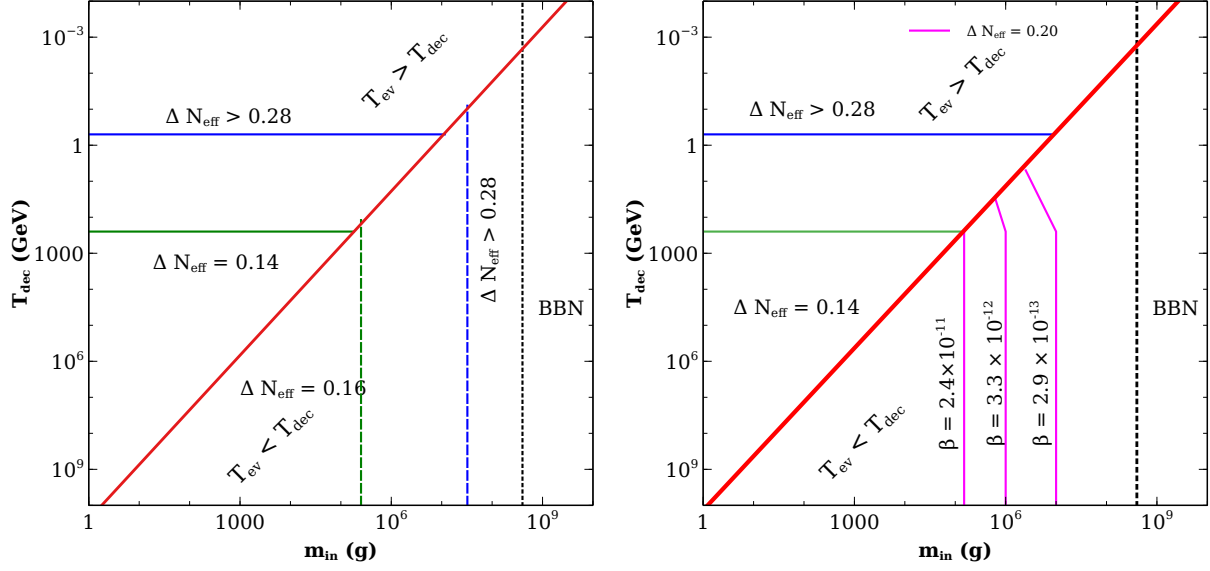


FIG. 2: ΔN_{eff} contours in the plane of initial PBH mass versus decoupling temperature. Here, we consider the extra light species X to be ν_R . The left plot is for the case where PBH dominate the energy density at the time of evaporation, whereas in the right panel, PBH energy density is always less than that of radiation. The black vertical dashed line indicates the upper bound on PBH mass from BBN limit.

2. PBH evaporation after decoupling of thermalised DR

Next, we consider the scenario where PBH evaporates after the thermal decoupling of species X . In this case, ΔN_{eff} can, in principle, get contributions from both sources. We can write

$$\Delta N_{\text{eff}} = \Delta N_{\text{eff}}^{\text{BH}} + \Delta N_{\text{eff}}^{\text{th}}, \quad (20)$$

where the first term on the right hand side (RHS) denotes the contribution from PBH and the second term indicates the thermal contribution. Now, for PBH domination, evaporation of PBH will lead to entropy injection to the thermal bath. Thus the thermal contribution from X to ΔN_{eff} gets diluted. Taking into account the effect of dilution, the above equation for Dirac active neutrinos can be written as

$$\Delta N_{\text{eff}} = 0.772 \frac{g_*(T_{\text{ev}})}{(g_{*s}(T_{\text{ev}}))^{4/3}} + 0.14175 \times \left(\frac{106.75}{g_*(T_{\text{dec}})} \right)^{4/3} \xi^{-4/3}, \quad (21)$$

where the parameter ξ quantifies decrease in ΔN_{eff} due to entropy dilution. It can be written as the ratio of the comoving entropy density at PBH evaporation (T_{ev}) to that at thermal

decoupling of X (T_{dec})

$$\xi = \frac{S_{\text{ev}}}{S_{\text{dec}}} = \frac{g_{*s}(T_{\text{ev}})a^3(T_{\text{ev}})T_{\text{ev}}^3}{g_{*s}(T_{\text{dec}})a^3(T_{\text{dec}})T_{\text{dec}}^3}. \quad (22)$$

Without any entropy injection, conservation of entropy gives $\xi = 1$. For entropy injection due to PBH evaporation, we have $\xi > 1$. It turns out that for PBH dominated region, $\xi \gg 1$, diluting the contribution from thermal ν_R or X in general. Thus, one can safely neglect the second term in the RHS of Eq. (20). Hence, only the X from PBH will contribute to ΔN_{eff} . PBH mass greater than around 4×10^7 g leads to ΔN_{eff} greater than the Planck 2σ bound, as shown earlier (cf. left panel of Fig. 1).

B. Radiation domination

If the ratio of the initial energy density of PBH to that of radiation energy density is less than β_{crit} , the early universe remains dominated by radiation only. Similar to the PBH-dominated universe, we can also have the same two scenarios, namely $T_{\text{ev}} > T_{\text{dec}}$ and $T_{\text{ev}} < T_{\text{dec}}$. The solid red line in the right panel plot of Fig. 2 corresponds to $T_{\text{dec}} = T_{\text{ev}}$. We discuss the two scenarios corresponding to either side of this solid red line below.

1. PBH evaporation before decoupling of thermalised DR

Similar to the case of PBH domination, here the thermal contribution is the only contributing factor to ΔN_{eff} . Hence the region and bounds are same as that of PBH domination, as already discussed in III A 1.

2. PBH evaporation after decoupling of thermalised DR

Here, the total contribution to ΔN_{eff} can be written in the form of Eq. (20), with the non-thermal contribution $\Delta N_{\text{eff}}^{\text{BH}}$ given by Eq. (16). $\Delta N_{\text{eff}}^{\text{BH}}$ is evaluated by solving the Boltzmann equations (9)-(11). Unlike the case of PBH domination, here the contribution from the thermalised DR can not be neglected as the entropy injection is negligible (i.e. $\xi \sim 1$) for $\beta < \beta_{\text{crit}}$. Hence, ΔN_{eff} will bear contribution from both thermalised as well as PBH generated DR. Also, for PBH domination, $\Delta N_{\text{eff}}^{\text{BH}}$ is independent of the parameter β , whereas in the present scenario β plays a significant role. The role of β can be seen from

the magenta coloured lines shown in the right panel plot of Fig. 2. The magenta coloured lines denote a total $\Delta N_{\text{eff}} = 0.20$. As the initial mass of PBH increases, its contribution to ΔN_{eff} also increases. As a result, one needs to reduce the value of β to get same ΔN_{eff} . Let us consider the magenta line with $m_{\text{in}} = 10^7$ g. The straight vertical portion of the line indicates a thermal contribution of 0.14 and a PBH contribution of 0.06. The contribution from PBH can be set to the required value by adjusting β . Decreasing T_{dec} in the right panel plot up to ~ 200 GeV leads to no changes in the thermal contribution as g_{*s} remain constant, giving a constant contribution to $\Delta N_{\text{eff}}^{\text{th}}$. Decreasing T_{dec} below ~ 200 GeV, the thermal contribution increases due to the reasons discussed earlier. So, one requires a smaller contribution of $\Delta N_{\text{eff}}^{\text{BH}}$ in order to maintain a total contribution of 0.20. This can be done by either decreasing PBH mass or by decreasing β . Here we decrease the PBH mass keeping β constant. This leads to the bending of magenta lines for $T_{\text{dec}} < 200$ GeV.

C. Summary of results

Now let us look at the combined results of PBH and radiation domination in the β - m_{in} plane. In the PBH dominated case, the magenta-shaded region in Fig. 3 shows the portion of parameter space where $\Delta N_{\text{eff}} > 0.28$, corresponding to PBH initial mass $m_{\text{in}} \gtrsim 4 \times 10^7$ g (cf. blue-dashed contour of left panel plot in Fig. 2). Now, this constraint is only valid if ν_R (or DR, in general) decouples from the bath before PBH evaporation i.e. if $T_{\text{dec}} > 150$ MeV (intersection of the blue dashed contour with the solid red line in left panel plot of Fig. 2). If ν_R decouples after PBH evaporation, then ΔN_{eff} will bear contribution from thermalised ν_R (existing thermal $\nu_R + \nu_R$ from PBH that will also get thermalised). In such a case, no constraint on the PBH parameters β or m_{in} can be obtained, since the contribution is purely thermal.

In the radiation-dominated region, if the thermalised ν_R decouples earlier, then even for very small β , one expects minimum contribution of $\Delta N_{\text{eff}}^{\text{th}} = 0.14$ to ΔN_{eff} . For example, let us fix $T_{\text{dec}} \approx 35$ GeV. So, for PBH mass greater than $\sim 7 \times 10^5$ g, the decoupling of ν_R occurs before PBH evaporation. The thermal contribution to ΔN_{eff} is about ≈ 0.17 . So, if the PBH contribution to ΔN_{eff} is more than 0.11, the total ΔN_{eff} would exceed 0.28. The blue shaded region in Fig. 3 denotes the area for which $\Delta N_{\text{eff}} > 0.28$. Note that there is a discontinuity between the magenta and blue shaded regions. This is because,

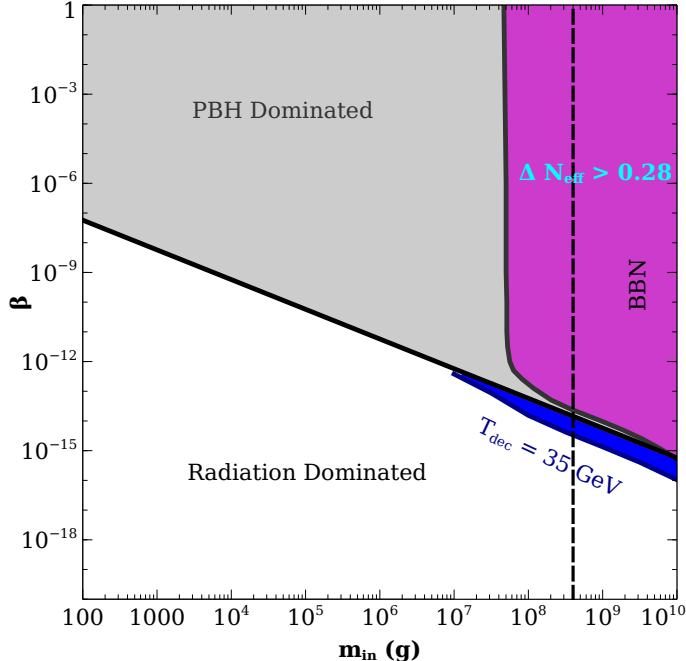


FIG. 3: ΔN_{eff} contours in the β - m_{in} plane. The magenta and blue region are the portion for PBH and radiation domination respectively where $\Delta N_{\text{eff}} > 0.28$. The black vertical dashed line indicates the upper bound on PBH mass from BBN limit.

we have assumed that in the PBH dominated era, the thermal contribution to ΔN_{eff} will be totally diluted away due to subsequent PBH evaporation and hence can be neglected. However, in the vicinity of the solid red line, i.e. $\beta \sim \beta_{\text{crit}}$, the dilution would be smaller leading to a non-negligible thermal contribution which should be counted for. At the same time, for the radiation-dominated case, we have assumed no entropy dilution for the thermal contribution, which is not completely true in the vicinity of $\beta \sim \beta_{\text{crit}}$. This is due to the fact that even a sub-dominant but sizeable abundance of PBH can lead to some entropy dilution, howsoever small. All these intricacies will be taken care of when we explicitly solve the relevant Boltzmann equations by properly taking into account the entropy dilution factor near the transition region from PBH to radiation domination, which we discuss below.

We perform a numerical analysis to evaluate the total contribution to ΔN_{eff} . For this purpose, we use the publicly available code FRISBHEE [26] to calculate the non-thermal contribution $\Delta N_{\text{eff}}^{\text{BH}}$, and to properly include the entropy dilution factor (cf. Eq. (22)), which goes into the calculation of the thermal contribution $\Delta N_{\text{eff}}^{\text{th}}$. For illustrative purposes, we consider the DR or the extra light species X to be of three types namely, (i) ν_R , (ii)

Goldstone boson and (iii) massless gauge boson.

1. *Dirac neutrino*

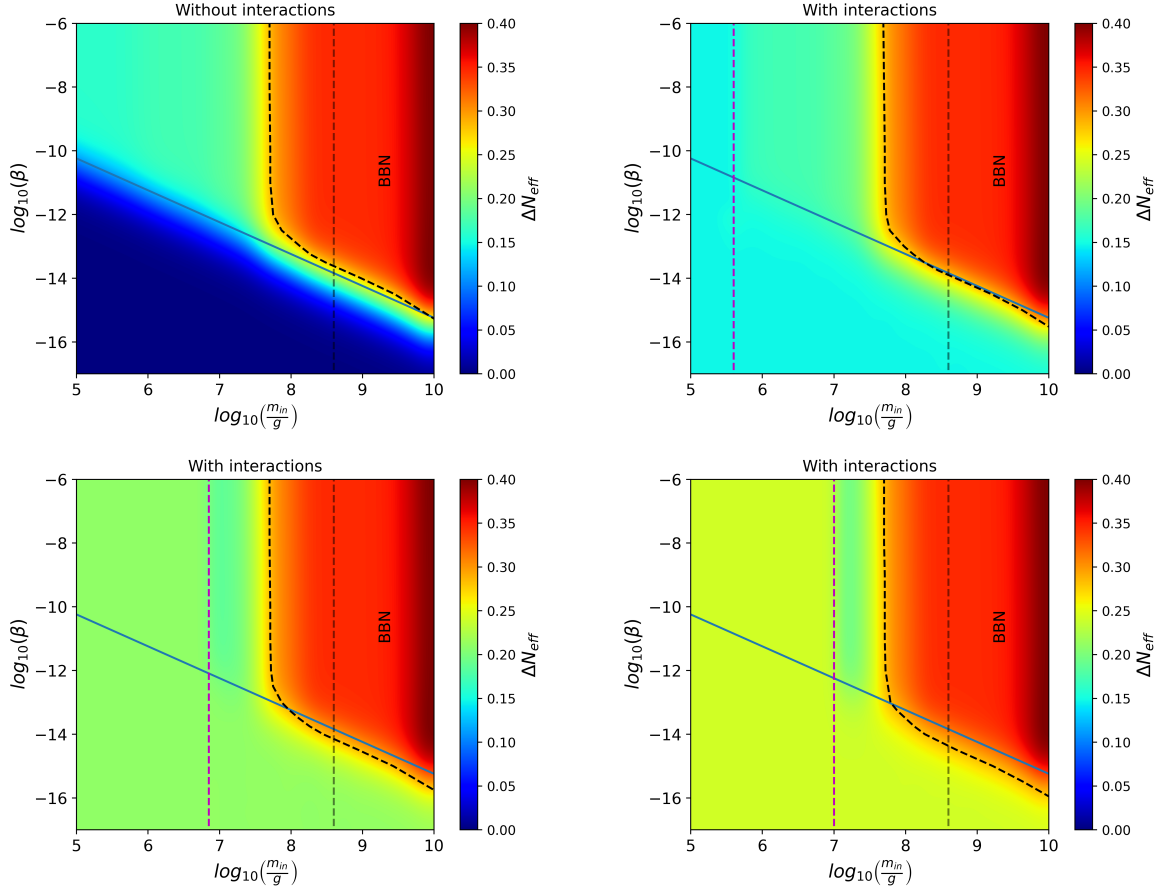


FIG. 4: *Dirac neutrino* : Variation of ΔN_{eff} in the m_{in} versus β plane for four different scenarios related to Dirac neutrinos: without any extra interactions of ν_R (top left panel), with interactions giving $\Delta N_{\text{eff}}^{\text{th}} = 0.14$, $T_{\text{dec}} = 100$ GeV (top right panel), $\Delta N_{\text{eff}}^{\text{th}} = 0.21$, $T_{\text{dec}} = 1$ GeV (bottom left panel) and $\Delta N_{\text{eff}}^{\text{th}} = 0.24$, $T_{\text{dec}} = 850$ MeV (bottom right panel) respectively. The regions right to the black dashed line indicate $\Delta N_{\text{eff}} > 0.28$ ruled out by Planck 2018 data at 2σ level. The dashed blue vertical line separates the regions $T_{\text{dec}} < T_{\text{ev}}$ and $T_{\text{dec}} > T_{\text{ev}}$ (not applicable to the top left panel due to no DR-SM interactions). The grey vertical dashed line indicates the upper bound on PBH mass from BBN limit.

Here, we consider 3 species of ν_R as the extra light degrees of freedom, as in usual Dirac active neutrino scenarios. In Fig. 4, we show the total contribution to ΔN_{eff} in

the $m_{\text{in}} - \beta$ plane for four different sub-cases. In the top left panel, we show the results where ν_R is produced purely from PBH due to negligible interactions with the SM bath. The black dashed contour corresponds to $\Delta N_{\text{eff}} = 0.28$, the maximum allowed by Planck 2018 data at 2σ level. This plot can be taken as a reference to compare the results in the presence of extra interactions. In the top right panel of Fig. 4, we show the results when the contribution from thermal ν_R is $\Delta N_{\text{eff}}^{\text{th}} \sim 0.147$. For this particular value of $\Delta N_{\text{eff}}^{\text{th}}$, the decoupling temperature should be $T_{\text{dec}} \gtrsim 100$ GeV corresponding to PBH mass $m_{\text{in}} \sim 4 \times 10^5$ g. PBH masses greater than $\sim 4 \times 10^5$ g, will evaporate later satisfying $T_{\text{ev}} < T_{\text{dec}}$. The vertical dashed line distinguishes these two regions. For $\beta \gg \beta_{\text{crit}}$, there is no change on the Planck 2018 bound compared to the results without interactions as the contribution of thermally decoupled species is negligible because of entropy dilution from PBH evaporation. However, near $\beta \sim \beta_{\text{crit}}$, i.e. the transition region between PBH and radiation domination, we can see a decrease albeit small in the values of β required to produce the same value of ΔN_{eff} as in the case without interactions. This is because near the boundary of the transition region, the effect of the thermal contribution starts appearing, and hence we need a lower value of β such that the non-thermal contribution $\Delta N_{\text{eff}}^{\text{BH}}$ decreases, resulting in a similar value of the total ΔN_{eff} . This explains slight lowering of the black-dashed contour corresponding to $\Delta N_{\text{eff}} = 0.28$. Note that the minimum contribution of the thermal species is 0.147, which is visible as we depart from the transition region. This is in sharp contrast to the results without interactions, where the value of ΔN_{eff} fades away to zero as we move deeper into the radiation domination ballpark. In the bottom panel, we have $\Delta N_{\text{eff}}^{\text{th}} = 0.21$ (left) and 0.24 (right). Due to the higher values of $\Delta N_{\text{eff}}^{\text{th}}$, and hence a lower decoupling temperature, the dashed vertical line shifts to the right corresponding to higher values of PBH mass (lower T_{ev}). Here, the change in the transition region is more apparent, due to a decrease in the contribution from PBH namely, $\Delta N_{\text{eff}}^{\text{BH}}$. We can see that for $\Delta N_{\text{eff}}^{\text{th}} = 0.24$, much more parameter space near the transition region is ruled out by current Planck 2018 data compared to that in the case without interactions (cf. top left panel of Fig. 4).

2. Goldstone boson

Let us consider the extra light species to be a Goldstone boson, a massless scalar. From Fig. 1 discussed before, we can see that the maximum contribution of Goldstone boson

produced solely from evaporating PBH to ΔN_{eff} is 0.10, which is below the Planck 2018 limit. However, it comes under the sensitivity of future experiments like CMB-S4. The top left panel plot of Fig. 5 shows the bound on ΔN_{eff} without any interaction. Unlike the case of ν_R , here the region to the right of the black dashed contour represents $\Delta N_{\text{eff}} > 0.06$, the CMB-S4 sensitivity as Planck 2018 data do not rule out any region of the parameter space at 2σ level. The top right panel and the bottom panel plots show the corresponding bounds with interactions between GB and SM. In the top right panel plot, the decoupling temperature is $T_{\text{dec}} = 100$ GeV and in the bottom panel plot, decoupling temperature is $T_{\text{dec}} = 1$ GeV. These correspond to $\Delta N_{\text{eff}}^{\text{th}} = 0.028$ and 0.042 respectively. Similar to the previous situation, a lower decoupling temperature gives a stronger constraint on the β versus m_{in} plane.

3. Massless gauge boson

From Fig. 1 discussed earlier, it can be seen that in the absence of PBH, the contribution of thermalised massless gauge boson to ΔN_{eff} is within the future CMB-S4 sensitivities for decoupling temperature $T_{\text{dec}} \lesssim 100$ GeV. As a result, a wide range of interactions of MGB with SM for which $T_{\text{dec}} \lesssim 100$ GeV can be probed by future CMB experiment like CMB-S4 (cf. right panel of Fig. 1). On the other hand, if PBH dominates in the early universe, the contribution to ΔN_{eff} always remains beyond the reach of future sensitivities, as shown in Fig. 1 (left panel). Thus, even if CMB-S4 rules out large coupling between MGB and SM which would produce large ΔN_{eff} , such large couplings (or equivalently lower T_{dec}) would still be allowed if we consider PBH domination in the early universe. This would be possible if we consider that PBH evaporates after the decoupling of MGB and sufficiently dilutes the thermal contribution.

IV. AN EXAMPLE: THERMALISED DIRAC NEUTRINO IN THE PRESENCE OF PBH

In the previous sections, we have studied the consequence of thermalised DR in the presence of PBH while considering different examples of DR as well as PBH parameters corresponding to both PBH and radiation domination in the early universe. However, we

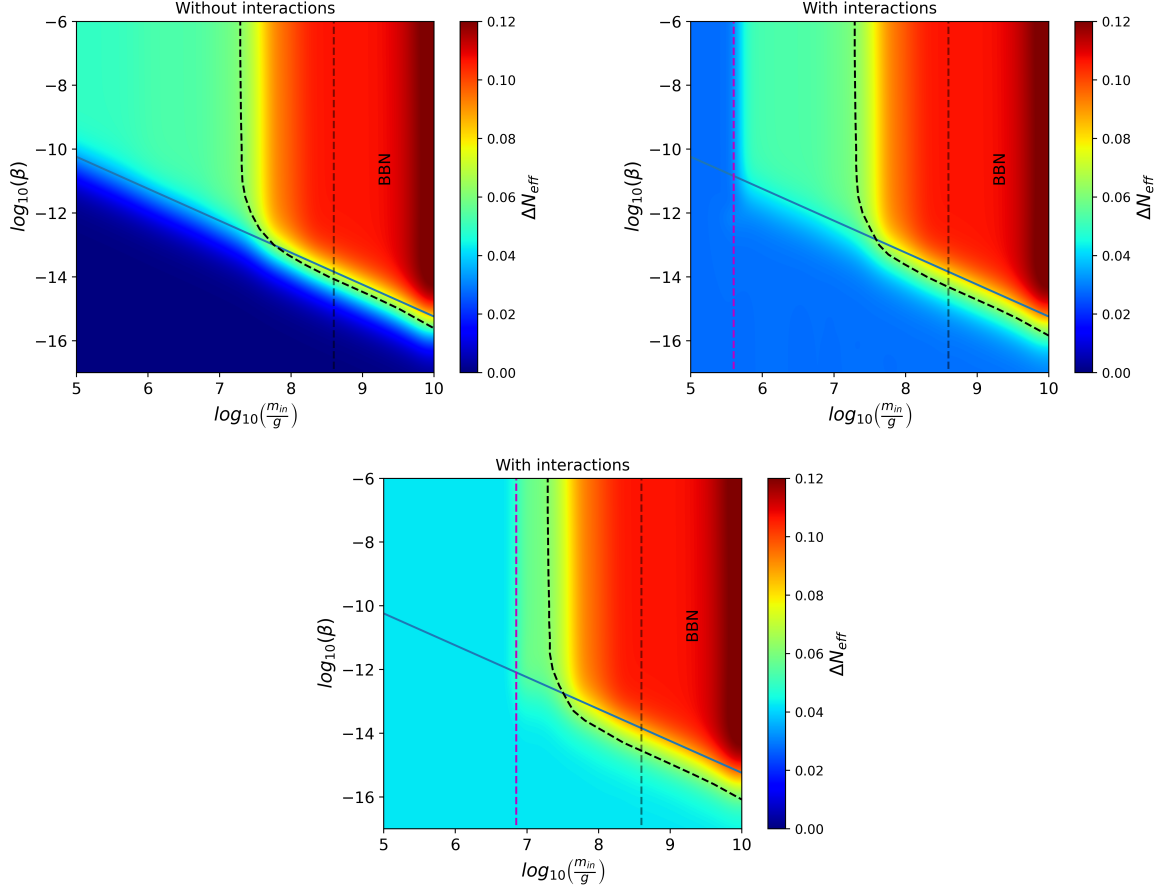


FIG. 5: *Goldstone boson* : Variation of ΔN_{eff} in the m_{in} versus β plane for three different scenarios related to Goldstone boson: without any extra interactions (top left panel), with interactions giving $\Delta N_{\text{eff}}^{\text{th}} = 0.028$, $T_{\text{dec}} = 100$ GeV (top right panel) and $\Delta N_{\text{eff}}^{\text{th}} = 0.042$, $T_{\text{dec}} = 1$ GeV (bottom panel) respectively. The regions right to the black dashed contour indicate $\Delta N_{\text{eff}} > 0.06$, the CMB-S4 sensitivity. The dashed blue vertical line separates the regions $T_{\text{dec}} < T_{\text{ev}}$ and $T_{\text{dec}} > T_{\text{ev}}$. The grey vertical dashed line indicates the upper bound on PBH mass from BBN limit.

discussed our results only in terms of decoupling temperatures of thermalised DR while being agnostic about the type of interactions with the SM bath. In this section, we consider a specific type of DR namely, light Dirac neutrinos and discuss our results for effective four-Fermi type interactions with the SM parametrised by the coupling parameter G_{eff} . Enhancement of ΔN_{eff} in Dirac neutrino models (without PBH) have been studied in several recent works [42–57].

The SM extended by three right-handed singlet Dirac neutrinos with Yukawa interactions $\mathcal{L}_Y = -Y_\nu^{ab} \bar{\ell}_L^a \tilde{\Phi} \nu_{bR}$, can explain tiny neutrino mass of $\mathcal{O}(\text{eV})$, with $Y_\nu \sim 10^{-12}$ as a result

of electroweak symmetry breaking induced by the SM Higgs doublet Φ . However, such small interactions can not thermalise the ν_R . Due to the smallness of Yukawa coupling, the non-thermal or freeze-in contribution to ΔN_{eff} from ν_R also remains negligible [49]. Thermalisation of ν_R may be possible in the presence of non-standard interactions which we consider to be of four-Fermi type interactions with the SM neutrinos ν_L [46] (see appendix A for details). This allows us to work in a model-independent manner while constraining the effective interactions as well as PBH parameters. The total interaction rate of ν_R arising from such four-fermion operators can be written as

$$\begin{aligned}\Gamma &= n_R^{\text{eq}} \langle \sigma v \rangle \\ &\simeq \frac{3}{4} \frac{\zeta(3)}{\pi^2} 2T^3 \frac{1}{4\pi} 4(3.151T)^2 G_{\text{eff}}^2,\end{aligned}\tag{23}$$

where G_{eff} is given by

$$G_{\text{eff}}^2 = \frac{4}{3}(G_S - 12G_T)^2 + \frac{5}{12}(\tilde{G}_S - 2G_V)^2,\tag{24}$$

where $G_S, \tilde{G}_S, G_T, G_V$ are dimensionful couplings involved in different four-fermion operators involving ν_R and ν_L as shown in appendix A. The equilibrium number density is denoted by n_R^{eq} . Comparing this interaction rate Γ with the Hubble rate of expansion (given by Eq. (12) and obtained by solving the Boltzmann equations (9)-(11)), we can find the decoupling temperature of ν_R . Note that the Hubble parameter contains contributions from both SM radiation and PBH, which can lead to a change in the ν_R decoupling temperature compared to the standard case without PBH.

With this, we redraw the Fig. 2 by replacing T_{dec} in the y-axis with the equivalent G_{eff} . The resulting plots are shown in Fig. 6 and Fig. 7 for PBH and radiation domination respectively. In the left panel plot of Fig. 6, the coupling G_S is non-zero while the rest (i.e. G_T, \tilde{G}_S and G_V) are zero. In the right panel plot, G_T is non-zero and the rest are set to zero. For $G_{\text{eff}} \gtrsim 10^{-3}G_F$ with G_F being the Fermi coupling, the decoupling temperature of ν_R turns to be $\lesssim 500$ MeV and ΔN_{eff} is more than 0.28. Similarly, below a certain value of coupling, $G_{\text{eff}} \sim 2 \times 10^{-7}G_F$, the contribution to ΔN_{eff} saturates at a value of 0.14. The corresponding parameter space is shown for the case of radiation domination in Fig. 7, which can be understood in a way analogous to the right panel plot of Fig. 2 discussed earlier.

Now, in order to check whether the right-handed neutrinos produced after PBH evaporation enters into thermal equilibrium with the SM bath, we calculate the interaction of ν_L

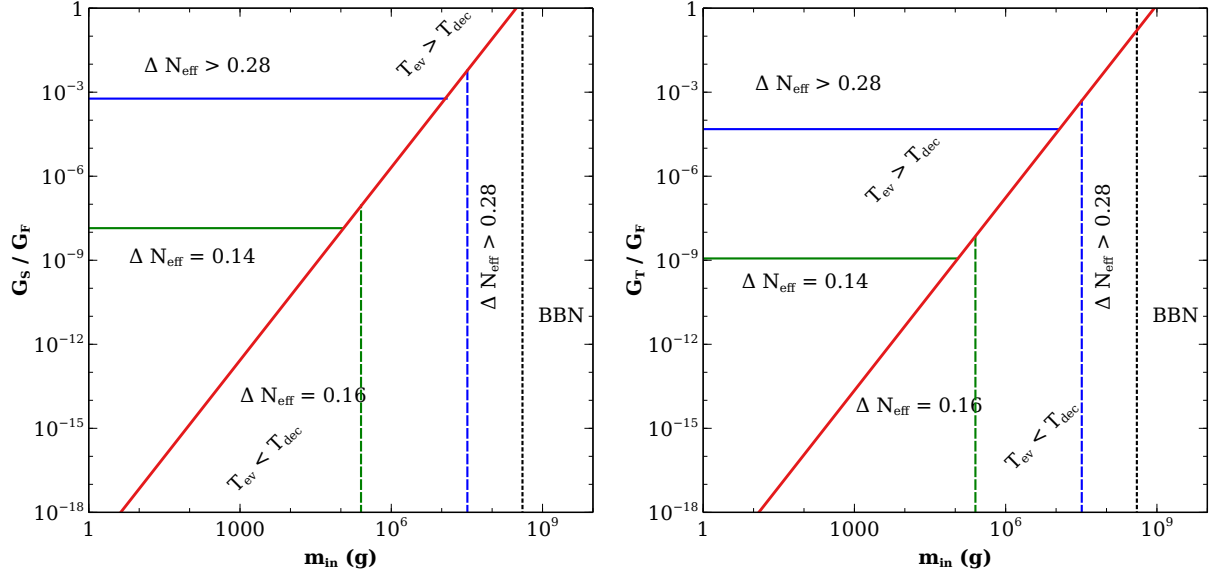


FIG. 6: ΔN_{eff} contours in the plane of initial PBH mass versus the effective neutrino coupling for the case of PBH domination. In the left panel, $G_T = \tilde{G}_S = G_V = 0$ with non-zero G_S , whereas in the right panel, we consider $G_S = \tilde{G}_S = G_V = 0$ with non-zero G_T . The black vertical dashed line indicates the upper bound on PBH mass from BBN limit.

present in the bath and non-thermal ν_R produced from PBH evaporation. Following [58], the thermal averaged cross-section for two massless species having different temperatures is found to be

$$\langle \sigma v \rangle_{T_{\text{ev}} T_{\text{BH}}} = \frac{1}{32(T_{\text{ev}} T_{\text{BH}})^{5/2}} \int_0^\infty \sigma s^{3/2} K_1 \left(\frac{\sqrt{s}}{\sqrt{T_{\text{ev}} T_{\text{BH}}}} \right) ds, \quad (25)$$

with K_1 being the modified Bessel's function of order 1. For $\sigma = \frac{1}{4\pi} s G_{\text{eff}}^2$, this gives

$$\langle \sigma v \rangle_{T_{\text{ev}} T_{\text{BH}}} = \frac{6}{\pi} G_{\text{eff}}^2 T_{\text{ev}} T_{\text{BH}} \quad (26)$$

Comparing the interaction rate corresponding to the above cross-section with the Hubble leads to the thermalisation condition

$$\frac{n_{\nu_L}^{\text{eq}}(T_{\text{ev}}) \langle \sigma v \rangle_{T_{\text{ev}} T_{\text{BH}}}}{H(T_{\text{ev}})} = C \frac{6}{\pi} G_{\text{eff}}^2 T_{\text{ev}}^2 T_{\text{BH}} = 1, \quad (27)$$

where $C = \frac{3}{4} \zeta(3) \times 2 \times \sqrt{45} \times M_P / (\pi^2 \sqrt{4\pi^3 g_*(T_{\text{ev}})})$.

Both T_{ev} and T_{BH} are functions of m_{in} as can be seen from Eq.(6) and Eq. (3). In the left panel of Fig. 8, we show the parameter space in the $m_{\text{in}} - G_{\text{eff}}$ plane, where re-thermalisation

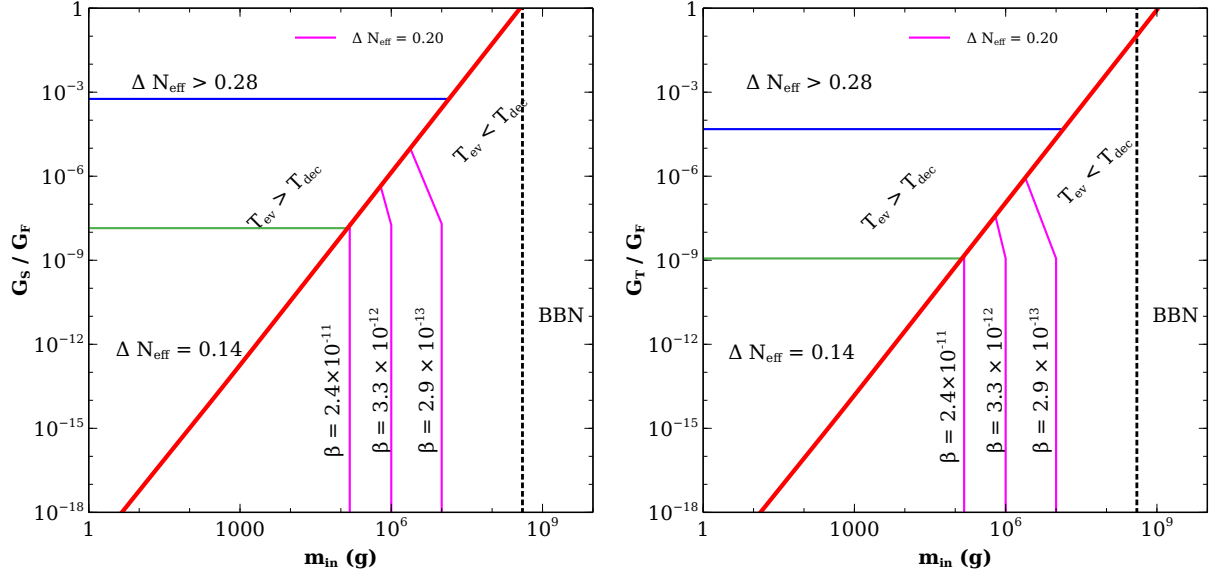


FIG. 7: ΔN_{eff} contours in the plane of initial PBH mass versus the effective neutrino coupling for the case of radiation domination. In the left panel, $G_T = \tilde{G}_S = G_V = 0$ with non-zero G_S , whereas in the right panel, we consider $G_S = \tilde{G}_S = G_V = 0$ with non-zero G_T . The black vertical dashed line indicates the upper bound on PBH mass from BBN limit.

of the PBH generated ν_R takes place (red-shaded), along with the region which does not lead to such re-thermalisation (blue-shaded). We can see that for a fixed PBH mass, if G_{eff} is smaller than a particular critical value, the non-thermally generated ν_R from PBH never thermalise again with the bath. A smaller value of G_{eff} also implies a higher initial decoupling temperature of thermal ν_R . Hence, it is also possible to relate this critical value of G_{eff} below which re-thermalisation does not occur, with the initial decoupling temperature of ν_R . In the right panel of Fig. 8, we show the parameter space in the $m_{\text{in}} - T_{\text{dec}}$ plane, separating the region of re-thermalisation from the rest. For a particular PBH mass, a decoupling temperature higher than $T_{\text{dec}}^{\text{crit}}$ leads to the situation where ν_R from PBH will never re-thermalise with the bath ⁴.

⁴ Considering a radiation dominated universe during decoupling, the value of this critical decoupling temperature is found to be

$$T_{\text{dec}}^{\text{crit}} \simeq (T_{\text{ev}}^2 T_{\text{BH}})^{1/3}. \quad (28)$$

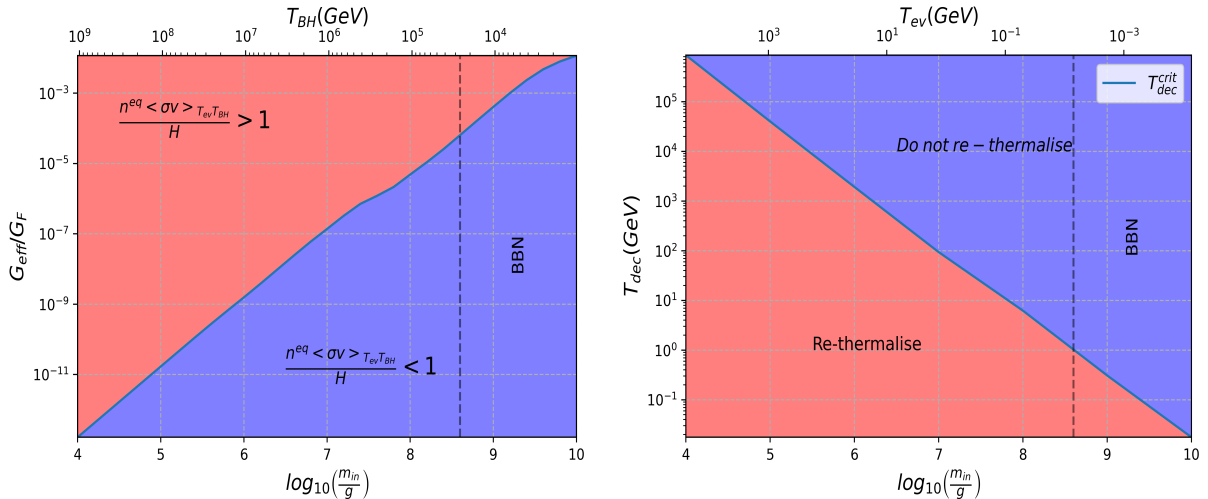


FIG. 8: *Left panel:* m_{in} versus G_{eff}/G_F parameter space showing the possibility of re-thermalisation. The red (blue) coloured region denotes the parameter space for which the PBH generated ν_R can (can not) come into thermal equilibrium. *Right panel:* m_{in} versus T_{dec} parameter space showing the possibility of re-thermalisation. The red and blue coloured regions have the same meaning as the ones in left panel plot. The vertical dashed line indicates the upper bound on PBH mass from BBN limit.

To summarise, Fig. 8 shows the constraints on the parameter space for which the ν_R produced from PBH evaporation will never re-thermalise. Once, we identify the parameter space where re-thermalisation occurs, the next step is to find the new ΔN_{eff} for these regions. However, this requires a careful treatment of complete Boltzmann equations to track the phase-space distribution function of evaporated ν_R , which is numerically expensive and out of the scope of the current work. Here, we assume that the new decoupling temperature of ν_R after re-thermalisation is $\sim T_{\text{ev}}$ for a particular PBH mass. This can be justified by the fact that PBH generated ν_R having a large initial energy and a sufficiently large interaction rate with the bath responsible for re-thermalisation, also suffer from instant dissipation of the energy to the bath. Due to this instant dissipation of energy, ν_R can not maintain equilibrium for a longer period after re-thermalisation leading to decoupling of ν_R once again at a temperature very close to T_{ev} .

With this, it is possible to find new constraint on G_{eff} and m_{in} . In the left panel of Fig. 9, constraints are shown in $m_{\text{in}}-G_{\text{eff}}$ plane. The black dashed lines denote $\Delta N_{\text{eff}} = 0.28$. Taking

into account re-thermalisation, it is possible to obtain a stronger constraint on $G_{\text{eff}}/G_{\text{F}}$. In the region, $T_{\text{dec}} < T_{\text{ev}}$, $\Delta N_{\text{eff}} > 0.28$ implies $G_{\text{eff}}/G_{\text{F}} \gtrsim 5 \times 10^{-4}$. However, in the re-thermalisation region, $G_{\text{eff}}/G_{\text{F}}$ up to $\sim 5 \times 10^{-7}$ can be excluded, for $m_{\text{in}} \gtrsim 10^{7.2}$ g. In the bottom triangular region, which shows the parameter space where PBH generated ν_R do not re-thermalise, the results correspond to the one discussed in Fig. 4. In this region, we have shown the ΔN_{eff} values for a particular value of $\beta = 10^{-8}$. In the right panel of Fig. 9, we show the constraint in the m_{in} versus β plane for a particular $G_{\text{eff}}/G_{\text{F}} = 10^{-6}$. Here, the region between the white dashed lines shows the parameter space leading to re-thermalisation. As expected from the left plot, here a stronger constraint on PBH mass can be seen.

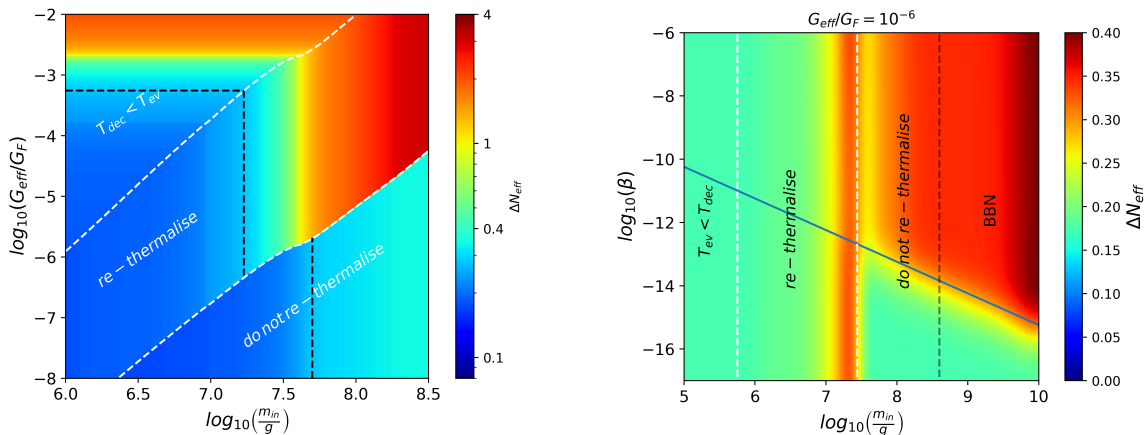


FIG. 9: *Left panel:* Variation of ΔN_{eff} in $m_{\text{in}}-G_{\text{eff}}/G_{\text{F}}$ plane for three different regions where (i) $T_{\text{dec}} < T_{\text{ev}}$, (ii) PBH generated ν_R re-thermalise and (iii) PBH generated ν_R do not re-thermalise, separated by white dashed line. The dashed black coloured line distinguishes the regions with $\Delta N_{\text{eff}} > 0.28$ and $\Delta N_{\text{eff}} < 0.28$. *Right panel:* Variation of ΔN_{eff} in the $m_{\text{in}}-\beta$ plane for a particular $G_{\text{eff}}/G_{\text{F}} = 10^{-6}$. A new constraint is obtained in the *re-thermalised* region. The black vertical dashed line indicates the upper bound on PBH mass from BBN limit.

V. GRAVITATIONAL WAVES FROM PBH DENSITY PERTURBATIONS

PBH can be involved in the generation of gravitational waves in several ways [59–61]. In this work, we focus on the gravitational waves induced by the density fluctuations of PBH after their formation [62–64]. This is primarily because for the PBH mass range we are

working with, the GW spectrum produced through this route can be within the sensitivity of near-future GW experiments. Moreover, these induced gravitational waves are independent of the formation mechanism of PBH.

After the formation of PBH, they are distributed randomly in space following Poissonian statistics [62]. These inhomogeneities in the distribution of PBH induce curvature perturbations when PBH begin to dominate the energy density of the universe, which at second order can source gravitational waves. The amplitude of these gravitational waves is further enhanced during the evaporation of PBH. The dominant contribution to the present-day GW amplitude can be written as⁵ [63, 66, 67]

$$\Omega_{\text{gw}}(t_0, f) \simeq \Omega_{\text{gw}}^{\text{peak}} \left(\frac{f}{f^{\text{peak}}} \right)^{11/3} \Theta(f^{\text{peak}} - f), \quad (29)$$

where $\Omega_{\text{gw}}^{\text{peak}}$ indicates the peak amplitude and is given by

$$\Omega_{\text{gw}}^{\text{peak}} \simeq 2 \times 10^{-6} \left(\frac{\beta}{10^{-8}} \right)^{16/3} \left(\frac{m_{\text{in}}}{10^7 \text{g}} \right)^{34/9}. \quad (30)$$

Now, for length scales smaller than the mean separation between PBH, the assumption of PBH as a continuous fluid ceases to hold true. This imposes an ultraviolet cutoff to the GW spectrum, with f^{peak} corresponding to comoving scales representing the mean separation between PBH. The peak frequency is found to be

$$f^{\text{peak}} \simeq 1.7 \times 10^3 \text{ Hz} \left(\frac{m_{\text{in}}}{10^4 \text{g}} \right)^{-5/6}. \quad (31)$$

Since GW behave like radiation, they can contribute to extra relativistic degrees of freedom during BBN. This gives an upper bound on β , depending on PBH mass, which is given by [63]

$$\beta \lesssim 1.1 \times 10^{-6} \left(\frac{m_{\text{in}}}{10^4 \text{g}} \right)^{-17/24}. \quad (32)$$

This upper bound on β for ultralight PBH is stronger than other bounds, obtained for eg. in Ref. [62] to avoid the backreaction problem.

Now, if PBH play a role in sourcing the extra relativistic degrees of freedom ΔN_{eff} , then the peak amplitude and the peak frequency of the GW spectrum discussed above would

⁵ The amplitude of the induced GW spectrum is sensitive to the PBH mass distribution [65]. Here, we consider a monochromatic mass spectrum for simplicity, as mentioned earlier.

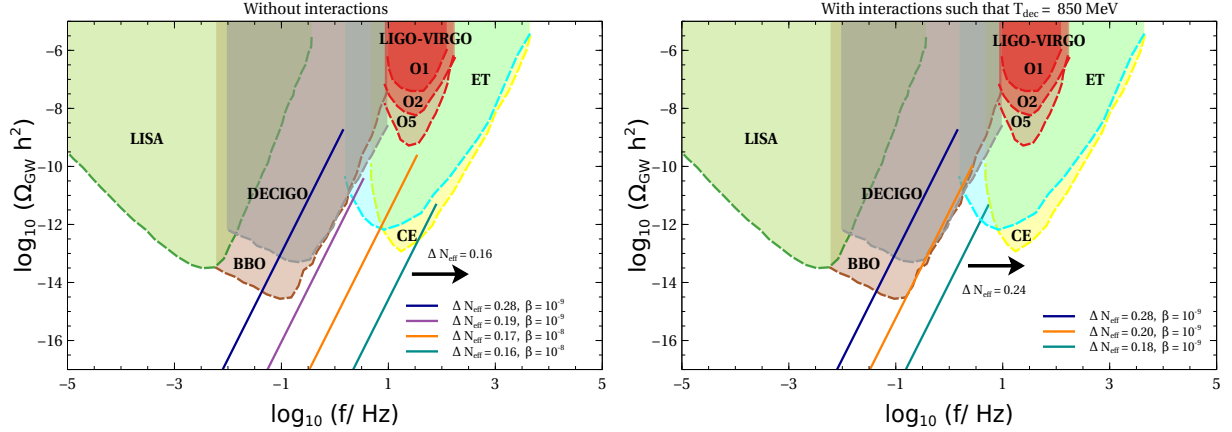


FIG. 10: GW spectra from PBH density fluctuations for different values of ΔN_{eff} , without extra interactions (left panel) and in the presence of extra interactions (right panel) of right-handed neutrinos. The various shaded regions indicate the future sensitivities and current bounds of GW detectors which includes LISA, BBO, DECIGO, LIGO-VIRGO, ET, CE. The arrows indicate a constant ΔN_{eff} beyond a particular frequency (see text).

depend on the value of ΔN_{eff} , since m_{in} in Eq. (30), (31) is connected to ΔN_{eff} , as we have already seen in earlier discussions. Hence, observation of such a GW spectrum would provide a complementary probe to ΔN_{eff} observations at CMB experiments. In the left panel of Fig. 10, we show the GW spectrum arising from PBH density fluctuations, for different values of ΔN_{eff} , in the absence of extra interactions of the right-handed neutrinos. Note that such a GW spectrum is absent for the radiation-dominated case. For PBH domination, a higher value of ΔN_{eff} corresponds to a higher value of m_{in} (cf. Fig. 1), which shifts the peak frequency given by Eq. (31) to lower values. Any spectral line to the right of the one coloured in dark cyan, would correspond to the same value of $\Delta N_{\text{eff}} \simeq 0.16$, since PBH masses in that range evaporate above the electroweak scale, giving the same value of ΔN_{eff} (see Fig. 1). Here, β remains a free parameter as for PBH domination, ΔN_{eff} is independent of β . In the right panel of Fig. 10, we show the GW spectra in the presence of extra interactions of right-handed neutrinos, with the strength of the interactions taken such that the thermal ν_R decouple at a temperature of ~ 850 MeV. This case corresponds to the bottom right panel of Fig. 4. Here, any spectral line to the right of the one coloured in dark cyan, would correspond to the same value of $\Delta N_{\text{eff}} = 0.24$, since PBH in this mass range evaporate at a temperature higher than 850 MeV. Thus, the thermal contribution would dominate as

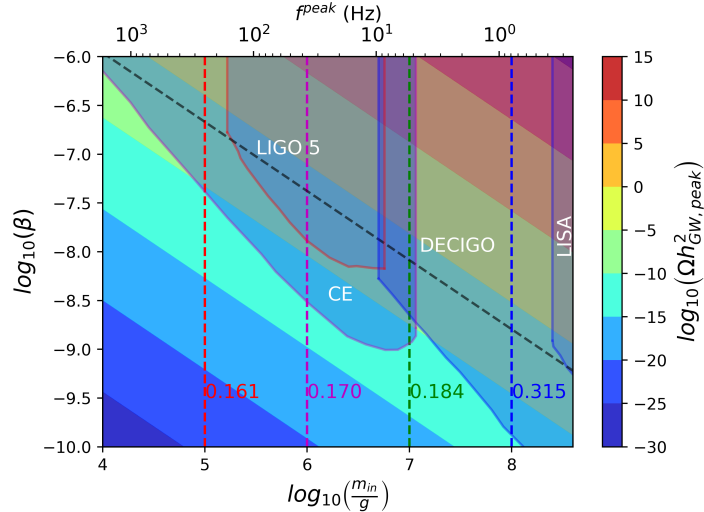


FIG. 11: Contours of peak amplitude of GW induced by PBH density perturbations. The corresponding ΔN_{eff} due to PBH generated ν_R are shown assuming no (or very feeble) ν_R -SM interactions. The black dashed line indicates the upper bound on β (cf. Eq. (32)).

discussed earlier, contributing to a total ΔN_{eff} of 0.24, similar to the bottom right panel of Fig. 4. In both the plots shown in Fig. 10, the experimental sensitivities of relevant GW detectors namely, LISA [68], DECIGO [69], BBO [70], ET [71], CE [72] and LIGO-VIRGO [73] are shown.

As we have seen already, the value of ΔN_{eff} is independent of β for PBH domination. Thus, future observations of N_{eff} from CMB observations will not be able to tell us anything about β provided $\beta > \beta_{\text{crit}}$. However, the value of β can be inferred from future GW detection with the spectral shape similar to the one generated by PBH density perturbations, since the peak of the GW amplitude is determined by β . In Fig. 11, we show the contours of the peak amplitude of GW in the $m_{\text{in}} - \beta$ plane, indicating the values of f_{peak} and ΔN_{eff} , considering no extra interactions of ν_R with the SM. The future sensitivities of several GW experiments are also shown in the same figure. In the presence of extra interactions, the values of ΔN_{eff} would be different as discussed above (cf. Fig. 10). ΔN_{eff} values would also be different for other light species. Finally, we summarise the GW and CMB complementarities in table I and II by choosing a few benchmark points. PBH mass and initial energy fraction are fixed at benchmark values and the corresponding implications for ΔN_{eff} and GW observations for different types of dark radiation namely, ν_R , Goldstone boson, massless gauge boson are

TABLE I: Without DR-SM interaction

BP	m_{in} (g)	β	ΔN_{eff}			CMB experiment (2σ)			GW experiment
			ν_R	GB	MGB	ν_R	GB	MGB	
BP1	10^6	1.5×10^{-8}	0.167	0.052	0.023	CMB-S4	CMB-HD	None	CE, ET, LIGO-VIRGO
BP2	10^7	6×10^{-9}	0.183	0.056	0.024	CMB-S4	CMB-HD	None	CE, ET, DECIGO, BBO
BP3	10^8	6×10^{-10}	0.313	0.096	0.042	Planck	CMB-S4	CMB-HD	DECIGO, BBO

TABLE II: With DR-SM interaction

BP	m_{in} (g)	β	T_{dec} (GeV)	ΔN_{eff}			CMB experiment (2σ)			GW experiment
				ν_R	GB	MGB	ν_R	GB	MGB	
BP1	10^6	1.5×10^{-8}	10	0.188	0.035	0.072	CMB-S4	CMB-HD	CMB-S4	CE, ET, LIGO-VIRGO
BP2	10^7	6×10^{-9}	0.8	0.242	0.046	0.092	CMB-S4	CMB-HD	CMB-S4	CE, ET, DECIGO, BBO
BP3	10^8	6×10^{-10}	0.01	3.02	0.575	1.15	Planck	Planck	Planck	DECIGO, BBO

shown in table I and II. Note that we work with β values consistent with the upper bound given by Eq. (32), and higher than the critical value β_{crit} (cf. Eq. (7)) required for PBH to dominate. While in table I, no DR-SM interactions are assumed, in table II, thermalised DR is considered with specific decoupling temperatures. While BP1 and BP2 in both the cases remain within future sensitivities, BP3 for some specific type of DR is already ruled out by Planck 2σ limits.

VI. CONCLUSION

We revisit the prospects of generating dark radiation from primordial black holes in the early universe, by considering sizeable DR-SM interactions. We first reproduce the results by considering PBH and thermal interactions separately and the consequences for ΔN_{eff} observations at CMB experiments. We then consider the hybrid scenario with both thermal interactions and PBH to be source of DR and put new constraints on the PBH parameters as well as DR-SM interactions from the requirement of satisfying BBN and CMB limits on ΔN_{eff} . Compared to the scenario with no DR-SM interactions discussed in earlier works, our present scenario puts tighter constraints on the PBH parameter space namely, initial PBH mass and energy density.

We also find an interesting region of parameter space involving PBH as well as DR-SM interactions where DR initially decouples from the bath followed by PBH evaporation leading to re-thermalisation of DR with the SM bath. This leads to a lower decoupling temperature of DR enhancing the ΔN_{eff} and putting new constraints in the PBH parameter space. Though we have considered a specific type of DR namely, light Dirac neutrinos for the numerical analysis, the generic conclusions are applicable to any thermalised DR.

We also find the gravitational wave complementarity of this scenario by considering PBH density perturbations to be the source of such stochastic GW. In the ultra-light PBH window considered in our work, GW sourced from PBH this way not only remains within current and planned experiment's sensitivity but also remains independent of PBH formation mechanism. We show the complementarity between GW and CMB observations for different types of DR with and without DR-SM interactions. Interestingly, some of the benchmark points can lead to GW peak amplitude, frequency in LIGO-VIRGO ballpark while keeping ΔN_{eff} within the reach future CMB experiments like CMB-S4. On the contrary, some part of the parameter space can keep GW prospects within future experiment's reach while saturating Planck 2018 limits on ΔN_{eff} . Such complementary detection prospects at CMB and GW experiments of thermalised dark radiation is particularly interesting due to limited prospects of detecting such light degrees of freedom at particle physics experiments.

Before we end, we briefly comment on the impact of Kerr PBH and a non-monochromatic mass function of PBH. First of all, considering Kerr PBH does not significantly alter DR contribution to ΔN_{eff} . This is true for DR with spin 0, 1/2 and 1, but significant enhancement is observed for spin 2 DR particles [26, 74, 75]. At the same time, our results on the analysis of GW spectrum would almost be unchanged. This is mainly because the evaporation temperature of a spinning BH changes only slightly compared to the non-spinning case [76, 77]. On the other hand, ΔN_{eff} can depend significantly on the mass distribution of PBH. In Ref. [27], it was shown that the contribution to ΔN_{eff} might substantially change for some choices of the mass spectrum, compared to the monochromatic case. Similarly, the amplitude of induced GW is also sensitive to the PBH mass spectrum [65, 78]. It would be interesting to study the combined effect in the situation where DR is produced both from thermal bath (due to sizeable DR-SM couplings) and from PBH with non-monochromatic mass distribution and non-zero spin distribution. We leave such a complete study for future works.

Acknowledgements

ND would like to acknowledge Ministry of Education, Government of India for providing financial support for his research via the Prime Minister's Research Fellowship (PMRF) December 2021 scheme. SJD thanks Dibyendu Nanda for some useful discussions related to this project. The work of DB is supported by the Science and Engineering Research Board (SERB), Government of India grant MTR/2022/000575.

Appendix A: Non-standard interactions of dark radiation

We consider the following effective operators for interactions among SM neutrinos and ν_R [46].

$$\begin{aligned}
 -\mathcal{L} \supset & G_s \bar{\nu}_L \nu_R \bar{\nu}_L \nu_R + G_s^* \bar{\nu}_R \nu_L \bar{\nu}_R \nu_L + G_V \bar{\nu}_L \gamma^\mu \nu_L \bar{\nu}_R \gamma_\mu \nu_R + \tilde{G}_S \bar{\nu}_L \nu_R \bar{\nu}_R \nu_L \\
 & + G_T \bar{\nu}_L \sigma^{\mu\nu} \nu_R \bar{\nu}_L \sigma_{\mu\nu} \nu_R + G_T^* \bar{\nu}_R \sigma^{\mu\nu} \nu_L \bar{\nu}_R \sigma_{\mu\nu} \nu_L, \quad (\text{A1})
 \end{aligned}$$

where G_S, \tilde{G}_S, G_V and G_T are effective coupling constants of respective 4-fermion operators. The relevant processes which can lead to thermalisation of ν_R are given by

$$\begin{aligned}
 \nu_R + \nu_R & \leftrightarrow \nu_R + \nu_R, \\
 \nu_R + \bar{\nu}_R & \leftrightarrow \nu_L + \bar{\nu}_L, \\
 \nu_R + \nu_L & \leftrightarrow \nu_R + \nu_L, \\
 \nu_R + \bar{\nu}_L & \leftrightarrow \nu_R + \bar{\nu}_L, \\
 \nu_R + \bar{\nu}_L & \leftrightarrow \bar{\nu}_R + \nu_L. \quad (\text{A2})
 \end{aligned}$$

While we have focused on the case of right-handed neutrinos, interactions of other species of dark radiation with Standard Model can also be realised through effective operators. For example, coupling of Goldstone bosons (ϕ) with the SM gauge sector at dimension-5 can be written as [79]

$$\mathcal{L} \supset -\frac{1}{4} \frac{\phi}{\Lambda} \left(c_1 B_{\mu\nu} \tilde{B}^{\mu\nu} + c_2 W_{\mu\nu} \tilde{W}^{\mu\nu} + c_3 G_{\mu\nu} \tilde{G}^{\mu\nu} \right), \quad (\text{A3})$$

where $\{B_{\mu\nu}, W_{\mu\nu}, G_{\mu\nu}\}$ denotes the field strength tensor associated with SM gauge groups $\{U(1)_Y, SU(2)_L, SU(3)_c\}$, with $\{\tilde{B}^{\mu\nu}, \tilde{W}^{\mu\nu}, \tilde{G}^{\mu\nu}\}$ being their duals. Interaction of Goldstone bosons with the SM can also be realised through Yukawa couplings given by [79]

$$\mathcal{L} \supset -\frac{\partial_\mu \phi}{\Lambda_\psi} \bar{\psi}_1 \gamma^\mu (g_V^{ij} + g_A^{ij} \gamma^5) \psi_j, \quad (\text{A4})$$

where ψ denotes the SM fermions. Similar analysis performed in Section IV for Dirac neutrinos can be carried out to constrain the couplings of other species of dark radiation.

-
- [1] PARTICLE DATA GROUP collaboration, *Review of Particle Physics*, *PTEP* **2020** (2020) 083C01.
 - [2] PLANCK collaboration, *Planck 2018 results. VI. Cosmological parameters*, 1807.06209.
 - [3] L. Ackerman, M.R. Buckley, S.M. Carroll and M. Kamionkowski, *Dark Matter and Dark Radiation*, *Phys. Rev. D* **79** (2009) 023519 [0810.5126].
 - [4] D.N. Spergel and P.J. Steinhardt, *Observational evidence for selfinteracting cold dark matter*, *Phys. Rev. Lett.* **84** (2000) 3760 [astro-ph/9909386].
 - [5] S. Tulin and H.-B. Yu, *Dark Matter Self-interactions and Small Scale Structure*, *Phys. Rept.* **730** (2018) 1 [1705.02358].
 - [6] J.S. Bullock and M. Boylan-Kolchin, *Small-Scale Challenges to the Λ CDM Paradigm*, *Ann. Rev. Astron. Astrophys.* **55** (2017) 343 [1707.04256].
 - [7] R.H. Cyburt, B.D. Fields, K.A. Olive and T.-H. Yeh, *Big Bang Nucleosynthesis: 2015*, *Rev. Mod. Phys.* **88** (2016) 015004 [1505.01076].
 - [8] J.J. Bennett, G. Buldgen, P.F. De Salas, M. Drewes, S. Gariazzo, S. Pastor et al., *Towards a precision calculation of N_{eff} in the Standard Model II: Neutrino decoupling in the presence of flavour oscillations and finite-temperature QED*, *JCAP* **04** (2021) 073 [2012.02726].
 - [9] J. Froustey, C. Pitrou and M.C. Volpe, *Neutrino decoupling including flavour oscillations and primordial nucleosynthesis*, *JCAP* **12** (2020) 015 [2008.01074].
 - [10] K. Akita and M. Yamaguchi, *A precision calculation of relic neutrino decoupling*, *JCAP* **08** (2020) 012 [2005.07047].
 - [11] G. Mangano, G. Miele, S. Pastor, T. Pinto, O. Pisanti and P.D. Serpico, *Relic neutrino decoupling including flavor oscillations*, *Nucl. Phys. B* **729** (2005) 221 [hep-ph/0506164].
 - [12] E. Grohs, G.M. Fuller, C.T. Kishimoto, M.W. Paris and A. Vlasenko, *Neutrino energy transport in weak decoupling and big bang nucleosynthesis*, *Phys. Rev. D* **93** (2016) 083522 [1512.02205].
 - [13] P.F. de Salas and S. Pastor, *Relic neutrino decoupling with flavour oscillations revisited*, *JCAP* **1607** (2016) 051 [1606.06986].

- [14] M. Escudero Abenza, *Precision early universe thermodynamics made simple: N_{eff} and neutrino decoupling in the Standard Model and beyond*, *JCAP* **05** (2020) 048 [[2001.04466](#)].
- [15] M. Cielo, M. Escudero, G. Mangano and O. Pisanti, *N_{eff} in the Standard Model at NLO is 3.043*, [2306.05460](#).
- [16] K. Abazajian et al., *CMB-S4 Science Case, Reference Design, and Project Plan*, [1907.04473](#).
- [17] SPT-3G collaboration, *SPT-3G: A Next-Generation Cosmic Microwave Background Polarization Experiment on the South Pole Telescope*, *Proc. SPIE Int. Soc. Opt. Eng.* **9153** (2014) 91531P [[1407.2973](#)].
- [18] SIMONS OBSERVATORY collaboration, *The Simons Observatory: Science goals and forecasts*, *JCAP* **02** (2019) 056 [[1808.07445](#)].
- [19] CMB-HD collaboration, *Snowmass2021 CMB-HD White Paper*, [2203.05728](#).
- [20] D. Hooper, G. Krnjaic and S.D. McDermott, *Dark Radiation and Superheavy Dark Matter from Black Hole Domination*, *JHEP* **08** (2019) 001 [[1905.01301](#)].
- [21] C. Lunardini and Y.F. Perez-Gonzalez, *Dirac and Majorana neutrino signatures of primordial black holes*, *JCAP* **08** (2020) 014 [[1910.07864](#)].
- [22] M.J. Baker and A. Thamm, *Black hole evaporation beyond the Standard Model of particle physics*, *JHEP* **01** (2023) 063 [[2210.02805](#)].
- [23] M.J. Baker and A. Thamm, *Probing the particle spectrum of nature with evaporating black holes*, *SciPost Phys.* **12** (2022) 150 [[2105.10506](#)].
- [24] F. Schiavone, D. Montanino, A. Mirizzi and F. Capozzi, *Axion-like particles from primordial black holes shining through the Universe*, *JCAP* **08** (2021) 063 [[2107.03420](#)].
- [25] A. Arbey, J. Auffinger, P. Sandick, B. Shams Es Haghi and K. Sinha, *Precision calculation of dark radiation from spinning primordial black holes and early matter-dominated eras*, *Phys. Rev. D* **103** (2021) 123549 [[2104.04051](#)].
- [26] A. Cheek, L. Heurtier, Y.F. Perez-Gonzalez and J. Turner, *Redshift effects in particle production from Kerr primordial black holes*, *Phys. Rev. D* **106** (2022) 103012 [[2207.09462](#)].
- [27] A. Cheek, L. Heurtier, Y.F. Perez-Gonzalez and J. Turner, *Evaporation of Primordial Black Holes in the Early Universe: Mass and Spin Distributions*, [2212.03878](#).
- [28] N. Bhaumik, A. Ghoshal, R.K. Jain and M. Lewicki, *Distinct signatures of spinning PBH domination and evaporation: doubly peaked gravitational waves, dark relics and CMB complementarity*, *JHEP* **05** (2023) 169 [[2212.00775](#)].

- [29] T. Fujita, M. Kawasaki, K. Harigaya and R. Matsuda, *Baryon asymmetry, dark matter, and density perturbation from primordial black holes*, *Phys. Rev. D* **89** (2014) 103501 [[1401.1909](#)].
- [30] B. Carr, K. Kohri, Y. Sendouda and J. Yokoyama, *Constraints on Primordial Black Holes*, [2002.12778](#).
- [31] I. Masina, *Dark matter and dark radiation from evaporating primordial black holes*, *Eur. Phys. J. Plus* **135** (2020) 552 [[2004.04740](#)].
- [32] S.W. Hawking, *Particle Creation by Black Holes*, *Commun. Math. Phys.* **43** (1975) 199.
- [33] S. Hawking, *Gravitationally collapsed objects of very low mass*, *Mon. Not. Roy. Astron. Soc.* **152** (1971) 75.
- [34] W.H. Press and P. Schechter, *Formation of galaxies and clusters of galaxies by selfsimilar gravitational condensation*, *Astrophys. J.* **187** (1974) 425.
- [35] M. Braglia, A. Linde, R. Kallosh and F. Finelli, *Hybrid α -attractors, primordial black holes and gravitational wave backgrounds*, *JCAP* **04** (2023) 033 [[2211.14262](#)].
- [36] K. Kawana and K.-P. Xie, *Primordial black holes from a cosmic phase transition: The collapse of Fermi-balls*, *Phys. Lett. B* **824** (2022) 136791 [[2106.00111](#)].
- [37] T. Papanikolaou, *Primordial black holes in loop quantum cosmology: The effect on the threshold*, [2301.11439](#).
- [38] J.H. MacGibbon, *Quark and gluon jet emission from primordial black holes. 2. The Lifetime emission*, *Phys. Rev. D* **44** (1991) 376.
- [39] N. Bernal and O. Zapata, *Dark Matter in the Time of Primordial Black Holes*, *JCAP* **03** (2021) 015 [[2011.12306](#)].
- [40] PLANCK collaboration, *Planck 2018 results. X. Constraints on inflation*, *Astron. Astrophys.* **641** (2020) A10 [[1807.06211](#)].
- [41] PLANCK collaboration, *Planck 2018 results. VI. Cosmological parameters*, *Astron. Astrophys.* **641** (2020) A6 [[1807.06209](#)].
- [42] K.N. Abazajian and J. Heeck, *Observing Dirac neutrinos in the cosmic microwave background*, *Phys. Rev.* **D100** (2019) 075027 [[1908.03286](#)].
- [43] P. Fileviez Pérez, C. Murgui and A.D. Plascencia, *Neutrino-Dark Matter Connections in Gauge Theories*, *Phys. Rev.* **D100** (2019) 035041 [[1905.06344](#)].
- [44] D. Nanda and D. Borah, *Connecting Light Dirac Neutrinos to a Multi-component Dark Matter Scenario in Gauged $B - L$ Model*, [1911.04703](#).

- [45] C. Han, M. López-Ibáñez, B. Peng and J.M. Yang, *Dirac dark matter in $U(1)_{B-L}$ with Stueckelberg mechanism*, [2001.04078](#).
- [46] X. Luo, W. Rodejohann and X.-J. Xu, *Dirac neutrinos and N_{eff}* , *JCAP* **06** (2020) 058 [[2005.01629](#)].
- [47] D. Borah, A. Dasgupta, C. Majumdar and D. Nanda, *Observing left-right symmetry in the cosmic microwave background*, *Phys. Rev. D* **102** (2020) 035025 [[2005.02343](#)].
- [48] P. Adshead, Y. Cui, A.J. Long and M. Shamma, *Unraveling the Dirac Neutrino with Cosmological and Terrestrial Detectors*, [2009.07852](#).
- [49] X. Luo, W. Rodejohann and X.-J. Xu, *Dirac neutrinos and N_{eff} II: the freeze-in case*, [2011.13059](#).
- [50] D. Mahanta and D. Borah, *Low scale Dirac leptogenesis and dark matter with observable ΔN_{eff}* , [2101.02092](#).
- [51] Y. Du and J.-H. Yu, *Neutrino non-standard interactions meet precision measurements of N_{eff}* , [2101.10475](#).
- [52] A. Biswas, D. Borah and D. Nanda, *Light Dirac neutrino portal dark matter with observable ΔN_{eff}* , *JCAP* **10** (2021) 002 [[2103.05648](#)].
- [53] D. Borah, S. Mahapatra, D. Nanda and N. Sahu, *Type II Dirac Seesaw with Observable ΔN_{eff} in the light of W -mass Anomaly*, [2204.08266](#).
- [54] S.-P. Li, X.-Q. Li, X.-S. Yan and Y.-D. Yang, *Effective neutrino number shift from keV -vacuum neutrinophilic 2HDM*, [2202.10250](#).
- [55] A. Biswas, D.K. Ghosh and D. Nanda, *Concealing Dirac neutrinos from cosmic microwave background*, *JCAP* **10** (2022) 006 [[2206.13710](#)].
- [56] A. Biswas, D. Borah, N. Das and D. Nanda, *Freeze-in dark matter via a light Dirac neutrino portal*, *Phys. Rev. D* **107** (2023) 015015 [[2205.01144](#)].
- [57] D. Borah, P. Das and D. Nanda, *Observable ΔN_{eff} in Dirac Scotogenic Model*, [2211.13168](#).
- [58] A. Cheek, L. Heurtier, Y.F. Perez-Gonzalez and J. Turner, *Primordial Black Hole Evaporation and Dark Matter Production: II. Interplay with the Freeze-In/Out Mechanism*, [2107.00016](#).
- [59] R. Anantua, R. Easther and J.T. Giblin, *GUT-Scale Primordial Black Holes: Consequences and Constraints*, *Phys. Rev. Lett.* **103** (2009) 111303 [[0812.0825](#)].
- [60] J.L. Zagorac, R. Easther and N. Padmanabhan, *GUT-Scale Primordial Black Holes: Mergers*

- and *Gravitational Waves*, *JCAP* **06** (2019) 052 [[1903.05053](#)].
- [61] R. Saito and J. Yokoyama, *Gravitational wave background as a probe of the primordial black hole abundance*, *Phys. Rev. Lett.* **102** (2009) 161101 [[0812.4339](#)].
- [62] T. Papanikolaou, V. Vennin and D. Langlois, *Gravitational waves from a universe filled with primordial black holes*, *JCAP* **03** (2021) 053 [[2010.11573](#)].
- [63] G. Domènech, C. Lin and M. Sasaki, *Gravitational wave constraints on the primordial black hole dominated early universe*, *JCAP* **04** (2021) 062 [[2012.08151](#)].
- [64] G. Domènech, V. Takhistov and M. Sasaki, *Exploring evaporating primordial black holes with gravitational waves*, *Phys. Lett. B* **823** (2021) 136722 [[2105.06816](#)].
- [65] T. Papanikolaou, *Gravitational waves induced from primordial black hole fluctuations: the effect of an extended mass function*, *JCAP* **10** (2022) 089 [[2207.11041](#)].
- [66] D. Borah, S. Jyoti Das, R. Samanta and F.R. Urban, *PBH-infused seesaw origin of matter and unique gravitational waves*, *JHEP* **03** (2023) 127 [[2211.15726](#)].
- [67] B. Barman, D. Borah, S. Jyoti Das and R. Roshan, *Gravitational wave signatures of a PBH-generated baryon-dark matter coincidence*, *Phys. Rev. D* **107** (2023) 095002 [[2212.00052](#)].
- [68] LISA collaboration, *Laser Interferometer Space Antenna*, *arXiv e-prints* (2017) [arXiv:1702.00786](#) [[1702.00786](#)].
- [69] S. Kawamura et al., *The Japanese space gravitational wave antenna DECIGO*, *Class. Quant. Grav.* **23** (2006) S125.
- [70] K. Yagi and N. Seto, *Detector configuration of DECIGO/BBO and identification of cosmological neutron-star binaries*, *Phys. Rev. D* **83** (2011) 044011 [[1101.3940](#)].
- [71] ET COLLABORATION collaboration, *The einstein telescope: a third-generation gravitational wave observatory*, *Classical and Quantum Gravity* **27** (2010) 194002.
- [72] LIGO SCIENTIFIC collaboration, *Exploring the Sensitivity of Next Generation Gravitational Wave Detectors*, *Class. Quant. Grav.* **34** (2017) 044001 [[1607.08697](#)].
- [73] LIGO SCIENTIFIC collaboration, *Advanced LIGO*, *Class. Quant. Grav.* **32** (2015) 074001 [[1411.4547](#)].
- [74] D. Hooper, G. Krnjaic, J. March-Russell, S.D. McDermott and R. Petrossian-Byrne, *Hot Gravitons and Gravitational Waves From Kerr Black Holes in the Early Universe*, [2004.00618](#).

- [75] I. Masina, *Dark matter and dark radiation from evaporating Kerr primordial black holes*, [2103.13825](#).
- [76] R. Dong, W.H. Kinney and D. Stojkovic, *Gravitational wave production by Hawking radiation from rotating primordial black holes*, *JCAP* **10** (2016) 034 [[1511.05642](#)].
- [77] A. Arbey, J. Auffinger and J. Silk, *Evolution of primordial black hole spin due to Hawking radiation*, *Mon. Not. Roy. Astron. Soc.* **494** (2020) 1257 [[1906.04196](#)].
- [78] G. Domènech, *Scalar Induced Gravitational Waves Review*, *Universe* **7** (2021) 398 [[2109.01398](#)].
- [79] D. Baumann, D. Green and B. Wallisch, *New Target for Cosmic Axion Searches*, *Phys. Rev. Lett.* **117** (2016) 171301 [[1604.08614](#)].